atmosphere

MDPI

Article

Responses of Extreme Climates in South Asia under a G6sulfur Scenario of Climate Engineering

Jingrong Wang [1], Zhihua Zhang [1,*], M. James C. Crabbe [2,3] and Lipon Chandra Das [4]

1. Climate Modeling Laboratory, School of Mathematics, Shandong University, Jinan 250100, China
2. Wolfson College, Oxford University, Oxford OX2 6UD, UK
3. Institute of Biomedical and Environmental Science & Technology, University of Bedfordshire, Luton LU1 3JU, UK
4. Department of Mathematics, University of Chittagong, Chittagong 4331, Bangladesh

* Correspondence: zhangzhihua@sdu.edu.cn

Abstract: Under global warming scenarios, extreme climate events in South Asia will occur more frequently which will seriously threaten the safety of local residents. South Asia faces dual pressures of the obligation of carbon emissions reduction globally and the demand for a better life for huge populations. Stratospheric Aerosol Injection (SAI) climate engineering provides a potential solution to this dilemma. We compared the evolution of 12 climate extreme indices under historical scenarios, two future scenarios (SSP245, SSP585) and an implementation scenario of SAI climate engineering (G6sulfur). We showed that the intensity and frequency of extreme climates under a G6sulfur scenario would be significantly higher than those under historical scenarios, and that the difference in extreme climates under three scenarios (SSP245, SSP585, and G6sulfur) would be widely varying, with some indices being considerably mitigated while others would reflect a worse set of circumstances than would be the case without SAI climate engineering. Therefore, SAI climate engineering is not an effective tool to mitigate future climate extremes in South Asia under global warming scenarios.

Keywords: extreme climates; climate engineering; South Asia

check for updates

Citation: Wang, J.; Zhang, Z.; Crabbe, M.J.C.; Das, L.C. Responses of Extreme Climates in South Asia under a G6sulfur Scenario of Climate Engineering. *Atmosphere* **2023**, *14*, 1490. https://doi.org/10.3390/atmos14101490

Received: 12 August 2023
Revised: 23 September 2023
Accepted: 25 September 2023
Published: 26 September 2023

1. Introduction

Since the industrial revolution, anthropogenic carbon emissions have sharply increased, leading to an increase in the concentration of carbon dioxide in the atmosphere from ~280 ppm in the 1850s to ~418 ppm in 2023. During the same period, the global average surface temperature has increased by 0.8–1.3 °C. Various climate simulations reveal that the occurrence frequency and intensity of climate extremes and the resulting damage often increase exponentially and nonlinearly with surface temperature. In 2015, the Paris Agreement, jointly formulated by more than 190 countries worldwide, pointed out the need to maintain the changes in the global mean surface temperature within 2 °C by the end of the 21st century and to strive to maintain the warming amplitude within 1.5 °C, since a higher increase in temperature would result in a completely different planet than the one we have experienced over the last few millennia [1,2]. However, the latest IPCC AR6 special report indicated that, without significantly reducing carbon emissions, the goals of the Paris Agreement would not be achieved.

Carbon emission policies have always great uncertainty. In 2017, the US Trump administration made the decision to withdraw from the Paris Agreement due to so-called unfair economic burdens. It is very difficult to achieve the goal of controlling global warming solely through emission reduction measures. These concerns have led to calls for research on non-traditional mitigation strategies for achieving temperature control goals as an emergency response to global warming [3]. The large volcanic eruption on Mount Pinatubo in the Philippines in July 1991 ejected between 15–30 million tons of sulfur dioxide gas, with the result that the average temperature of the entire planet was cooled 0.4–0.5 °C.

Therefore, artificially increasing sulfate aerosols in the stratosphere (in short, Stratospheric Aerosol Intervention) was proposed as a climate engineering scheme, since it can increase the planetary albedo to reflect more sunlight back to space and induce a cooling that acts to partially offset global warming [4]. However, how much material would be necessary to produce the desired level of global mean cooling and how this would vary by injection altitude, latitude, and timing remains highly uncertain [5]. For implementation in the real world, SAI is generally considered the most plausible climate engineering scheme, at least for global applications, because of its low cost, plausible near-term readiness, large possible climate forcing, and relative safety [3,6]. This led to the known Stratospheric Controlled Perturbation Experiment (SCoPEx), which was the first real-world climate engineering test on the costs, benefits, and risks of a SAI climate engineering scheme.

Due to the potential side effects, risks, and uncertainty of climate engineering, the G6sulfur experiment in GeoMIP6 was proposed to simulate the use of Stratospheric Aerosol Intervention (SAI) to reduce the magnitude of the net anthropogenic radiative forcing from a high forcing scenario (SSP5-RCP8.5) to a moderate forcing scenario (SSP2-RCP4.5). Simulations in the G6sulfur experiment demonstrated that the SAI climate engineering scheme significantly mitigated the increase in global surface temperature [7]. All simulations indicated that SAI climate engineering has the potential to reduce global and local surface temperature increases. At the same time, with increasing injection rates in the 21st century, compared to the SSP585 scenario, SAI climate engineering would intensify the decrease in precipitation in southern Europe [7,8]. Such a reduction in both temperature and precipitation is mainly because the implementation of SAI climate engineering would alter temporal and spatial distributions of temperature change between day and night, between seasons, and between the tropics and the poles [9]. Jones et al. [4], further, found that the implementation of SAI climate engineering would force an increasingly positive phase of the North Atlantic Oscillation (NAO) as the injection rate increased over the course of the 21st century, and cause the Quasi-Biennial Oscillation (QBO) to stall and become locked in a phase with permanent westerly winds in the lower stratosphere [7]. Jones et al. [4] found that the zonal mean wind speed during Northern Hemisphere winter would have an increase of more than 9–12 m/s, and that the maximum increase would be centered over Alaska [4]. Tilmes et al. [10] found that the implementation of SAI climate engineering would result in a heating of the lower tropical stratospheric temperatures by 5–13 °C, further leading to changes in stratospheric transport and water vapor, as well as other related changes [10]. Tang et al. [11] revealed that SAI climate engineering would reduce the wildfire occurrence by decreasing the surface temperature and wind speed and increasing the relative humidity and soil water, with the exception of boreal regions where SAI climate engineering would increase the occurrence of wildfires due to a decrease in relative humidity and soil water compared with the present day [11]. Most SAI climate engineering research has focused on the global impacts, and limited regional impacts have been investigated in East Asia: Liu et al. [12] showed that SAI would intensify the Siberian high and Aleutian low, enhance the low-level northerly winds along the coast of East Asia, and deepen the East Asian trough during 2080–2099, reversing the weakening of EAWM under the SSP585 scenario (SSP5-8.5) [12]. Liang and Haywood (2023) found that SAI is effective at partly ameliorating the increases in atmospheric rivers (ARs) over the subtropical region of East Asia; however, it may result in more pronounced increases in ARs and associated precipitation over the upper midlatitude regions, particularly northeastern China [13]. Until now, the impacts of SAI climate engineering on climate extremes have not been investigated.

Different climatic conditions are spread over wide and diverse geographic regions of South Asia, including arid regions, low-lying coastal regions, alluvial plain regions, tropical regions, and mountainous regions. Due to outdated infrastructure and an agriculture-based economic system, South Asia is extremely sensitive and vulnerable to various climate extreme events: arid regions are threatened by severe drought events; low-lying coastal regions are threatened by sea level rise; alluvial plain regions are threatened by severe flooding; tropical regions are threatened by devastating cyclones; and mountainous regions are threatened by the retreat of glaciers. In view of atmospheric circulation, Due to being blocked by the Tibetan plateau in the north, the climate in South Asia is mainly dominated by Indian monsoons, and current and future climate change is making Indian monsoons more chaotic. South Asia always experiences heatwaves in the summers, but in recent years, heatwaves have arrived earlier and become more prolonged. Moreover, for every degree of warming, monsoon rainfalls will likely increase by about 5% [14]. Current and future climate change will lead to significant increases in the frequency and intensity of extreme climate events in South Asia, posing a serious threat to the lives of local residents [15]; especially, the heat stress could lead to a 50% reduction in the most high-yielding wheat area of the Indo-Gangetic River Plains [16]. Due to severe water scarcity, the GDP loss in South Asia is estimated to reach as high as 6% by 2050 [15]. Climate-induced damage frequently scales exponentially, rather than linearly, in terms of temperature and precipitation extremes. At the same time, there is growing recognition that the global mean temperature targets of 1.5 and 2 °C above pre-industrial would be extremely difficult to achieve under conventional mitigation scenarios. South Asia urgently needs to pursue a suitable approach to combat climate change and its related impacts. Meanwhile, South Asia faces dual pressures of the obligation of carbon emissions reduction globally and the demand for a better life for huge populations. SAI climate engineering provides a potential solution to this dilemma. Therefore, in this study, by making full use of the multi-model outputs of the G6sulfur experiment, we evaluate the possible mitigation performance of the frequency and intensities of extreme climates in South Asia under the implementation of SAI climate engineering schemes.

2. Data and Methods

Future climate evolutions are always predicted through scenario-based climate simulations. Shared Socioeconomic Paths (SSPs) consist of five projected socio-economic scenarios over the whole 21st century, including SSP1 (sustainable development), SSP2 (moderate development), SSP3 (local development), SSP4 (unbalanced development), and SSP5 (rapid development) [17]. Representative Concentration Pathways (RCPs) consist of four projected greenhouse gas concentrations scenarios with radiative forcing ranging from 2.6 to 8.5 W/m^2. Using the combination of SSPs and RCPs as plausible future scenarios in global climate simulations can make more reasonable predictions for further climate evolutions. The SSP245 scenario is a RCP4.5 global forcing pathway with SSP2 socioeconomic conditions, corresponding to moderate socioeconomic development and carbon emissions under government intervention; The SSP585 scenario is a RCP8.5 global forcing pathway with SSP5 socioeconomic conditions, corresponding to rapid socioeconomic development and high carbon emissions without government intervention [17].

The G6sulfur experiment has been designed to reflect a situation in which temperatures under a high-forcing future scenario (SSP585) are reduced to those under a medium-forcing scenario (SSP245) using the proposed geoengineering technique of stratospheric aerosol intervention (SAI). The criterion for comparing the G6sulfur and SSP245 simulations was initially defined by Kravitz et al. [8] in terms of radiative forcing, but this was subsequently altered to specify that the decadal global mean near-surface air temperatures of simulations under these two scenarios should be the same to within 0.2 °C [8]. The simulation experiment began in 2020 and continued until 2100. Due to the fact that excessive injection values in various climate models may result in highly variable results between models, the G6sulfur experiment only chose a moderate compulsion scenario as the target, rather than a low compulsion scenario [8]. Four global climate models (Table 1) have been used to run a G6sulfur experiment. These models (or their immediate forebears) have undergone various degrees of validation relevant to SAI using observations from explosive volcanic eruptions [4], so the reliability and robustness in G6sulfur simulations using these models have been accepted consistently by all researchers on SAI climate engineering. Direct analyses on the output of G6sulfur simulations by these models have been carried out widely since 2020 [4,6,10–14,18]. All models successfully reduce global mean surface air temperatures to within 0.2 °C of SSP245 levels on average throughout the century [18]; however, impacts of SAI climate engineering on climate extremes have not been investigated.

Table 1. Climate models used in this study.

Model	Institution	Resolution
CNRM-ESM2-1 [19]	CNRM-CERFACS, Toulouse, France	h: 256 × 128, v: 91
IPSL-CM6A-LR [20]	IPSL, Paris 75252, France	h: 144 × 143, v: 79
MPI-ESM1-2-LR [21]	MPI-M, Hamburg 20146, Germany	h: 192 × 96, v: 47
UKESM1-0-LL [22]	MOHC, Exeter, Devon, EX1 3PB, UK	h: 192 × 144, v: 85

Resolution is described as horizontal (h), lat × long, and vertical (v).

In order to study impacts of the SAI climate engineering scheme on extreme climate events, this study selected 12 widely used representative climate extreme indices (Table 2). These indices can represent difference aspects of climate extremes, from warm temperature extremes and cold temperature extremes to precipitation/drought extremes. Five indices (TXx, TNx, TXn, TNn, Rx1day) reveal extreme values in temperature and precipitation, while seven indices (SU, WSDI, ID, CSDI, CDD, CWD, Rx5day) reveal the duration of temperature/precipitation/drought extremes. SAI impacts on mean temperature and precipitation distributions in G6sulfur simulations have been shown to have significant regional differences in their simulations [4,18]. This means that impacts of SAI on different climate extreme indices are likely to be widely varying spatially over South Asia with some regions gaining considerably while others may be faced with a worse set of circumstances than would be the case without SAI. Therefore, we must analyze the spatial patterns and evolution trends of each climate extreme index in detail with/without SAI climate engineering implementation. In order to enhance the reliability, we calculated the evolution of 12 climate extreme indices by using an ensemble mean of four climate models (CNRM-ESM2-1 IPSL-CM6A-LR MPI-ESM1-2-LR UKESM1-0-LL) [19–22]. Comparing spatial patterns and trends of these climate extreme indices under four different scenarios (historical, SSP245, SSP585, and G6sulfur) by using the Mann-Kendall trend test and Sen's slope test, we revealed the possible role of SAI climate engineering in mitigating different types of extreme climates in South Asia.

Table 2. Definition of climate extreme indices.

Category	Index	Description	Definition	Unit
Warm Temperature Extremes	SU	Summer days	Annual number of days when TX > 25 °C	Days
	TXx	Highest Tmax	Annual maximum value of daily maximum temperature	°C
	TNx	Highest Tmin	Annual maximum value of daily minimum temperature	°C
	WSDI	Thermal endurance index	Annual count of days with at least six consecutive days when TX > 90th percentile	Days
Cold Temperature Extremes	ID	Ice days	Annual number of days when TX < 0 °C	Days
	TXn	Lowest Tmax	Annual maximum value of daily maximum temperature	°C
	TNn	Lowest Tmin	Annual minimum value of daily minimum temperature	°C
	CSDI	Cold persistence index	Annual count of days with at least six consecutive days when TN < 10th percentile	Days

Table 2. *Cont.*

Category	Index	Description	Definition	Unit
Precipitation Extremes	CDD	Consecutive dry days	Maximum number of consecutive days when precipitation < 1 mm	Days
	CWD	Consecutive wet days	Maximum number of consecutive days when precipitation ≥ 1 mm	Days
	Rx1day	Wettest consecutive one day	Maximum daily precipitation	mm
	Rx5day	Wettest consecutive five days	Maximum of consecutive 5-day (cumulative) precipitation amount	mm

TX: maximum temperature, TN: minimum temperature.

3. Study Area

South Asia is mainly located between the equator and the 30° north latitude. It is bounded to the north by the Hindu Kush, the Karakoram Range, and the Himalayas, and to the south by the Indian ocean (Figure 1). Geographically, the northern part of South Asia borders on the Himalayas, with significant vertical changes in climate, soil, and vegetation. The middle regions of South Asia are great plains which are formed by the alluvium of the Indus, Ganges, and Brahmaputra Rivers, and are some of the most fertile regions in the world [23]. Further south is the Deccan Plateau bordered by the Eastern and Western Ghats. In contrast to the abundant rainfall on both sides of the plateau, the interior of the plateau is hot with little rain [24].

Figure 1. Topographic Map of South Asia.

South Asia is mainly dominated by monsoonal climates. In dry seasons, during October–February, dry winds blow across South Asia from the northeast, while in the rainy season, during June-September, the winds blow from the southwest, bringing heavy rains, especially in the southwestern and Ganges Delta regions. Northwestern India and southern Pakistan are dominated by the Thar Desert and have a highly arid subtropical desert climate with a mean annual rainfall < 10 mm. This region lacks vegetation and is vulnerable to sand erosion [25]. From the Himalayas to fertile plains and coastal cities, due to its unique geographical location, South Asia is particularly vulnerable to extreme climates [26].

4. Results

In order to comprehensively understand the potential role of SAI climate engineering in mitigating extreme climates, we selected 12 representative climate extreme indices

(Table 2) and analyzed their evolution under four climate scenarios: historical (1985–2014), SSP245 (2030–2059), SSP585 (2030–2059), and G6sulfur (2030–2059). These indices can represent difference aspects of climate extremes, from warm temperature extremes and cold temperature extremes to precipitation/drought extremes. Five indices (TXx, TNx, TXn, TNn, Rx1day) reveal extreme values in temperature and precipitation, while seven indices (SU, WSDI, ID, CSDI, CDD, CWD, Rx5day) reveal the duration of temperature/precipitation/drought extreme events. Moreover, different climatic conditions are spread over wide and diverse geographic regions of South Asia, including arid regions, low-lying coastal regions, alluvial plain regions, tropical regions, and mountainous regions; therefore, we need to analyze the spatial patterns and evolution trends of each extreme index in detail with/without SAI climate engineering implementation.

4.1. SU Indices

SU indices measure the annual number of days with a daily maximum temperature > 25 °C. Under four climate scenarios (historical, SSP245, SSP585, and G6sulfur), the mean annual SU indices had similar spatial distribution patterns, and their values in the south Indian peninsula would be much higher than other regions in South Asia (Figure 2, first row). Due to the influence of the high altitude, southwest monsoons, and Westerlies, the lowest mean annual SU indices would always appear on the southern slope of the Himalayas. Under a historical scenario (1985–2014), the mean annual average SU index in India would be approximately 240–312 days. Regardless of the implementation of SAI climate engineering, under the scenarios of SSP245, SSP585, and G6sulfur, the mean annual SU indices from 2030 to 2059 would reach at most 262–318 days in the Deccan Plateau of India, while, with the increase in altitude, the mean annual SU index on the southern slope of the Himalayas would rapidly decrease to 74–180 days.

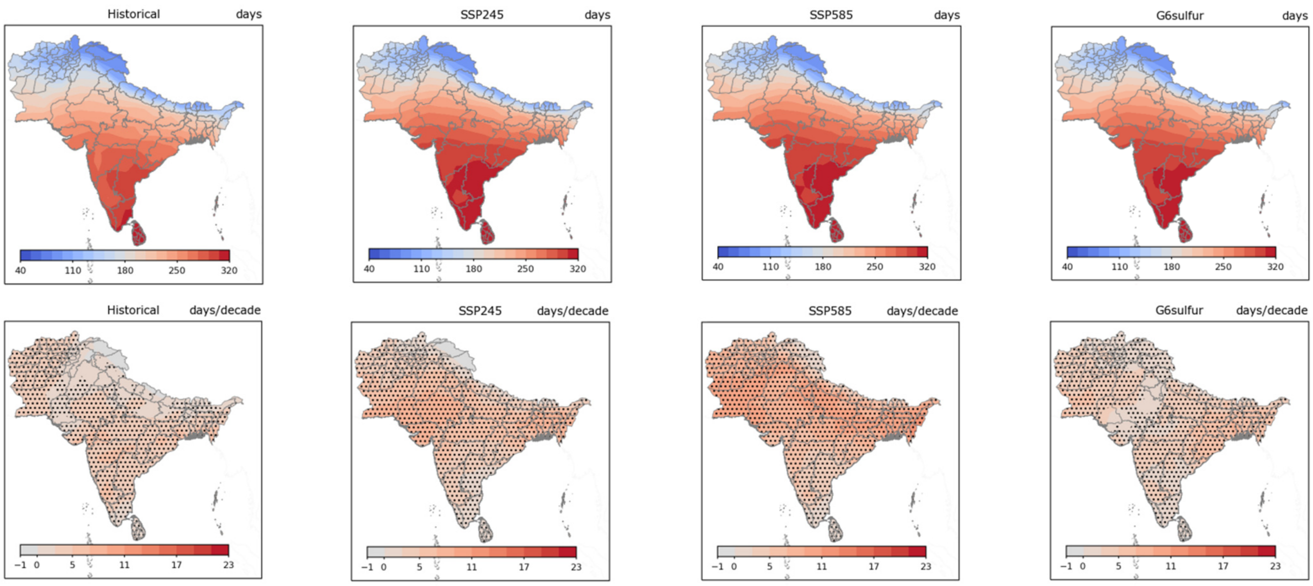

Figure 2. The first row shows mean annual SU indices under the four scenarios: historical (1985–2014), SSP245 (2030–2059), SSP585 (2030–2059), G6sulfur (2030–2059); The second row shows annual trend of SU indices under four scenarios: historical, SSP245, SSP585, G6sulfur, where stippling indicates statistically significant trends at a level $p < 0.05$.

Surrounded by a mountainous plateau, the Thar desert would become warmer under the SSP245 and G6sulfur scenarios, while Kashmir would have less warming due to the high altitude (Figure 2, first row). Under a SSP245 scenario, during 2030–2059, the mean annual SU indices in the Thar desert would be expected to be 13–37 days higher than those during 1985–2014, while these indices in Kashmir would be expected to be only 1–11 days higher than those during 1985–2014. Under the G6sulfur scenario, during 2030–2059, the mean annual SU indices of the Thar desert would be expected to be 15–35 days higher than those during 1985–2014, while the mean annual SU indices in Kashmir would be 1–13 days higher than those from 1985 to 2014. Compared with a SSP245 scenario, the G6sulfur scenario would decrease the mean annual SU indices in the Deccan Plateau by 1–4 days and increase the mean annual SU indices in other regions of South Asia by 1–3 days. Comparing a G6sulfur scenario with the SSP245 scenario, the G6sulfur scenario would show a significant mitigating warming effect on SU indices. During 2030–2059, compared with the SSP585 scenario, the G6sulfur scenario would have an additional decrease in the mean annual SU indices in the Indo-Gangetic Plains, Marva Plateau, and Thar desert by 1–7 days.

Under four climate scenarios (historical, SSP245, SSP585, and G6sulfur), the annual SU indices would have statistically significant increasing trends in most of South Asia (Figure 2, second row). Under the historical scenario (1985–2014), the annual SU indices in most of South Asia had an increasing trend (1–7 days/decade). Under the SSP245/SSP585 scenarios, the annual SU indices in the Indo-Gangetic Plains and the Thar desert would be predicted to have a more quickly increasing trend (up to 7–13 days/decade). Under the G6sulfur scenario, the annual SU indices would show a similar increasing trend to those under a historical scenario. The significant trend differences in annual SU indices among four scenarios for representative regions are shown in Table 3.

Table 3. Trend difference in SU index among four scenarios (Unit: days/decade).

Region \ Difference	SSP245-Historical	G6sulfur-Historical	G6sulfur-SSP245	G6sulfur-SSP585
Northern Afghanistan	−3 to −1	−2 to 0	−3 to 1	−5 to −2
Ganges River Plain	1 to 6	1 to 4	−4 to 1	−8 to 0
Interior of the Deccan Plateau	−3 to 0	−4 to −1	−4 to 1	−4 to 0
Thar desert	1 to 4	−1 to 2	−4 to 0	−7 to −2

4.2. WSDI Indices

The warm spell duration indices (WSDI) measure the annual count of days occurring during at least six consecutive days with a daily maximum temperature exceeding the 90th percentile threshold during 1985–2014. Under all scenarios, due to the influence of high altitude, the lowest mean annual WSDI index would appear on the southern slope of the Himalayas (Figure 3, first row). Under the historical scenario (1985–2014), the mean annual WSDI indices were always <14 days over the whole of South Asia, and their values in the Thar desert and the southern Indus River Plain were slightly higher than those in other regions in South Asia (Figure 3, first row). Regardless of the intervention of SAI climate engineering, under three future scenarios (SSP245, SSP585, and G6sulfur), the mean annual WSDI indices during 2030–2059 would exceed 45 days even in the southern slope of the Himalayas, and reach 75–205 days in the southern Deccan Plateau (Figure 3, first row). Under the SSP245 scenario (2030–2059), the mean annual WSDI indices in the Deccan Plateau would be 83–165 days higher than those during 1985–2014, while the mean annual WSDI indices in Afghanistan and Kashmir would be only 46–55 days higher. Under the G6sulfur scenario, during 2030–2059, the mean annual WSDI indices would be expected to be 91–178 days higher in the Deccan Plateau than those during 1985–2014, and 45–57 days higher in Afghanistan and Kashmir. Compared with the SSP245 scenario (2030–2059), the G6sulfur scenario would increase the mean annual WSDI indices by 7–15 days in the Deccan Plateau, by 1–7 days in the Thar Desert, and by 1–2 days in Afghanistan and Kashmir. Compared with the SSP585 scenario, the G6sulfur scenario would decrease the mean annual WSDI indices in the whole of South Asia by 6–23 days during 2030–2059; especially, by 12–23 days in the Deccan Plateau and 8–13 days in the west Ghats.

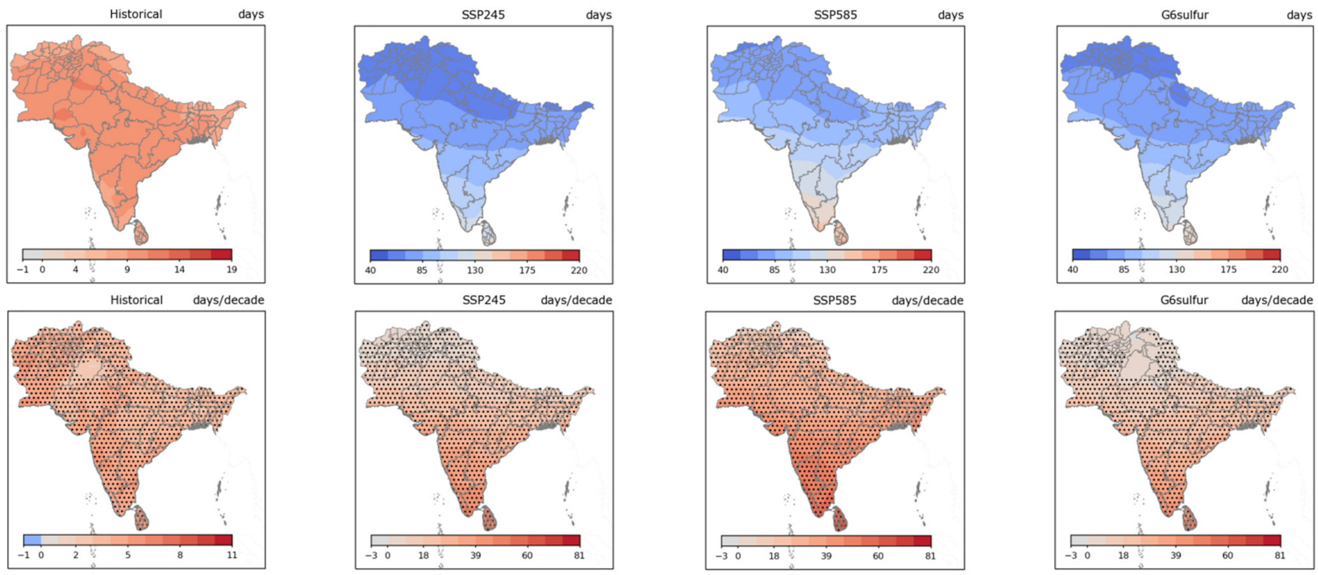

Figure 3. The first row shows mean annual WSDI indices under the four scenarios: historical (1985–2014), SSP245 (2030–2059), SSP585 (2030–2059), G6sulfur (2030–2059); the second row shows annual trend of WSDI indices under four scenarios: historical, SSP245, SSP585, G6sulfur, where stippling indicates statistically significant trends at a level $p < 0.05$.

The statistically significant increasing trends in the WSDI indices were detected over the whole of South Asia under all four scenarios (Figure 3, second row). Under the historical scenario (1985–2014), the annual WSDI indices had a slightly increasing trend (1–6 days/decade) in most of South Asia. Under the SSP245, SSP585, and G6sulfur scenarios, the annual WSDI indices demonstrated significant differences in annual trends: 0–20 days/decade in the northern regions and 60–80 days/decade in the southern regions. The significant trend difference in the WSDI indices among the four scenarios for representative regions are shown in Table 4.

Table 4. Trend difference in WSDI index among four scenarios (Unit: days/decade).

Difference / Region	SSP245-Historical	G6sulfur-Historical	G6sulfur-SSP245	G6sulfur-SSP585
Afghanistan	1 to 10	1 to 7	−5 to 2	−18 to −11
Western Ganges River Plain	8 to 19	8 to 14	−4 to −1	−16 to −8
Deccan Plateau	24 to 54	18 to 52	−10 to −1	−21 to −11
Kashmir	1 to 6	−2 to 5	−3 to 2	−14 to −7

4.3. TXx Indices

The TXx indices measure the annual maximum value of the daily maximum temperature. The spatial pattern of the mean annual TXx indices was similar under all four scenarios (Figure 4, first row). The Thar desert and its surroundings would always have much higher mean annual TXx indices than other regions of South Asia. With the increase in altitude, the lowest mean annual TXx index would always appear on the southern slope of the Himalayas. Under a historical scenario (1985–2014), except for northern Himalayan regions, the mean of the annual TXx indices in South Asia was approximately 30.5–40.9 °C (Figure 4, first row). Under the SSP245, SSP585, and G6sulfur scenarios, the mean annual TXx indices during 2030–2059 would have no significant difference, and the largest value would reach 35.4–42.1 °C in the western borders of South Asia and the lowest value would decline to 26.8–34.1 °C on the southern slope of the Himalayas. Since the warm South Asian monsoons are blocked by the Himalayas' ranges, the southern slope of the Himalayas would demonstrate stronger warming effects during future scenarios (SSP245 and G6sulfur), while the Deccan Plateau would demonstrate weaker warming effects due to its adjacency to the Indian Ocean and relative high altitudes. Under the SSP245 scenario (2030–2059), the mean annual TXx indices in Kashmir would be predicted to be 1.7–3.2 °C higher than the mean in the historical period (1985–2014), while these indices in the Deccan Plateau would be predicted to be only 0.3–1.6 °C higher. Under a G6sulfur scenario (2030–2059), the mean annual TXx indices in Kashmir would be predicted as 2.1–4.1 °C higher than those during 1985–2014, while the indices in the Deccan Plateau would be only 0.1–1.9 °C higher (Figure 4, first row). Compared with an SSP245 scenario, the G6sulfur scenario would increase the mean annual TXx indices on the southern slope of the Himalayas by 0.2–0.9 °C and in Kashmir by 0.3–0.8 °C. Due to adjacency to the Indian Ocean, the mean annual TXx indices in the southern Deccan Plateau were predicted to increase only by 0.1–0.2 °C. Compared to a SSP585 scenario, during 2030–2059, the G6sulfur scenario was predicted to decrease the mean annual TXx indices in most of the South Asian regions by 0.1–0.4 °C and increase them by a similar magnitude in the Indus river plain and Afghanistan.

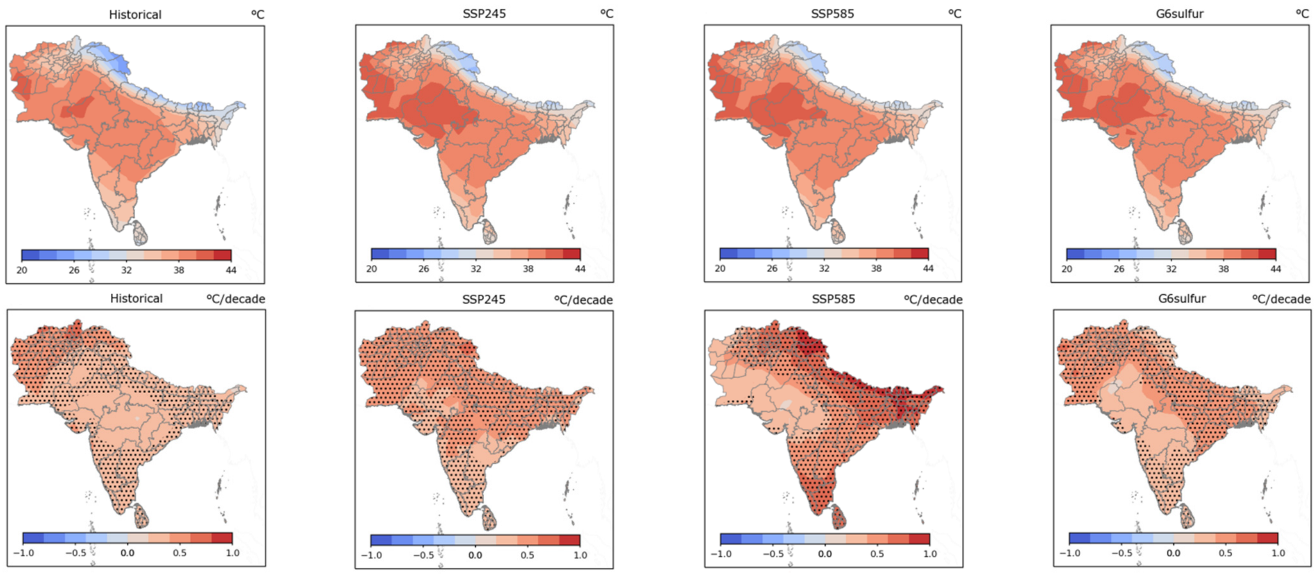

Figure 4. The first row shows mean annual TXx indices under the four scenarios: historical (1985–2014), SSP245 (2030–2059), SSP585 (2030–2059), G6sulfur (2030–2059); the second row shows annual trend of TXx indices under four scenarios: historical, SSP245, SSP585, and G6sulfur, where stippling indicates statistically significant trends at a level $p < 0.05$.

Under a historical scenario (1985–2014), except for the northern Deccan Plateau, the annual TXx indices in most of South Asia had a statistically significant increasing trend (0.2–0.7 °C/decade) (Figure 4, second row). Under the SSP245 scenario, the annual TXx indices in most South Asian regions would show a similar statistically significant increasing trend (0.1–0.7 °C/decade). Under the SSP585 scenario, except for the Sistan Basin in south Afghanistan, the southern Indus River Plain, the Thar desert, and the Malwa Plateau, the mean annual TXx indices in most regions of South Asia would show a statistically significant increasing trend (0.2–0.7 °C/decade). Under the G6sulfur scenario, except for the southeast Indus River Plain, Thar desert, and Malwa Plateau, the mean annual TXx indices in South Asia would show a statistically significant increasing trend (0.3–0.7 °C/decade). The significant trend difference in the annual TXx indices among four scenarios for representative regions are shown in Table 5.

Table 5. Trend difference in TXx index among four scenarios (Unit: °C/decade).

Region \ Difference	SSP245-Historical	G6sulfur-Historical	G6sulfur-SSP245	G6sulfur-SSP585
Eastern Afghanistan	−0.2 to 0.1	−0.3 to −0.1	−0.1 to 0	−0.2 to −0.1
The southern slope of the Himalayas	0.1 to 0.4	0 to 0.3	−0.3 to 0.4	−0.6 to 0
Western Deccan Platea	−0.2 to 0.2	−0.1 to 0.2	−0.4 to 0.1	−0.6 to −0.2
Western Indus River Plain	0 to 0.2	0.1 to 0.3	−0.3 to 0.4	0 to 0.2

4.4. TNx Indices

The TNx indices measure the annual maximum value of the daily minimum temperature. Under all four scenarios, the spatial pattern of the mean annual TNx indices was similar to the TXx indices; especially with the increase in altitude, the lowest mean annual TNx indices would always appear on the southern slope of the Himalayas (Figure 5, first row). Under the historical scenario (1985–2014), the mean annual TNx indices in most of South Asia were approximately 25.6–28.6 °C. Regardless of SAI climate engineering, under all three future scenarios, the mean annual TNx indices from 2030 to 2059 were predicted to have a slight increase to reach 26.9–30.1 °C in most regions of South Asia, but due to high altitude, the mean annual TNx indices on the southern slope of the Himalayas would only reach 18.6–21.1 °C. Compared with the historical scenario (1985–2014), the southern slope of the Himalayas and Kashmir would be much warmer during 2030–2059 than the Deccan Plateau. Under the SSP245 scenario, during 2030–2059, the largest increase in the mean annual TNx indices would occur in Kashmir (1.8–2.1 °C higher than those during 1985–2014). The increase in the mean annual TNx indices in other regions of South Asia would be similar (1–1.5 °C higher than that during 1985–2014). Under the G6sulfur scenario, the whole of South Asia would be warmer. Especially, during 2030–2059, the mean annual TNx indices in Kashmir would be 2.3–2.5 °C higher than those during 1985–2014. Compared with the SSP245 scenario, the G6sulfur scenario would further increase the mean annual TNx indices on the southern slope of the Himalayas by 0.3–0.6 °C and in the southern Deccan Plateau by 0–0.2 °C. At the same time, the mean annual TNx indices in the Marva Plateau would decrease by 0.1–0.3 °C. Compared with the SSP585 scenario, the G6sulfur scenario would decrease the mean annual TNx indices in the western Deccan Plateau, Marwa Plateau, and Thar desert by 0.3–0.5 °C during 2030–2059, and increase the mean annual TNx indices of the Ganges River Plain and its northern regions by 0–0.2 °C.

Under all four scenarios (historical, SSP245, SSP585, and G6sulfur), the annual TNx indices in the whole South Asian region would show a statistically significant increasing trend. Under the historical scenario, the increasing trend was about 0.2–0.6 °C/decade. Under three future scenarios, the increasing trends would be 0.2–0.9 °C/decade (Figure 5, second row). The significant trend difference in the annual TNx indices among four scenarios for representative regions are shown in Table 6.

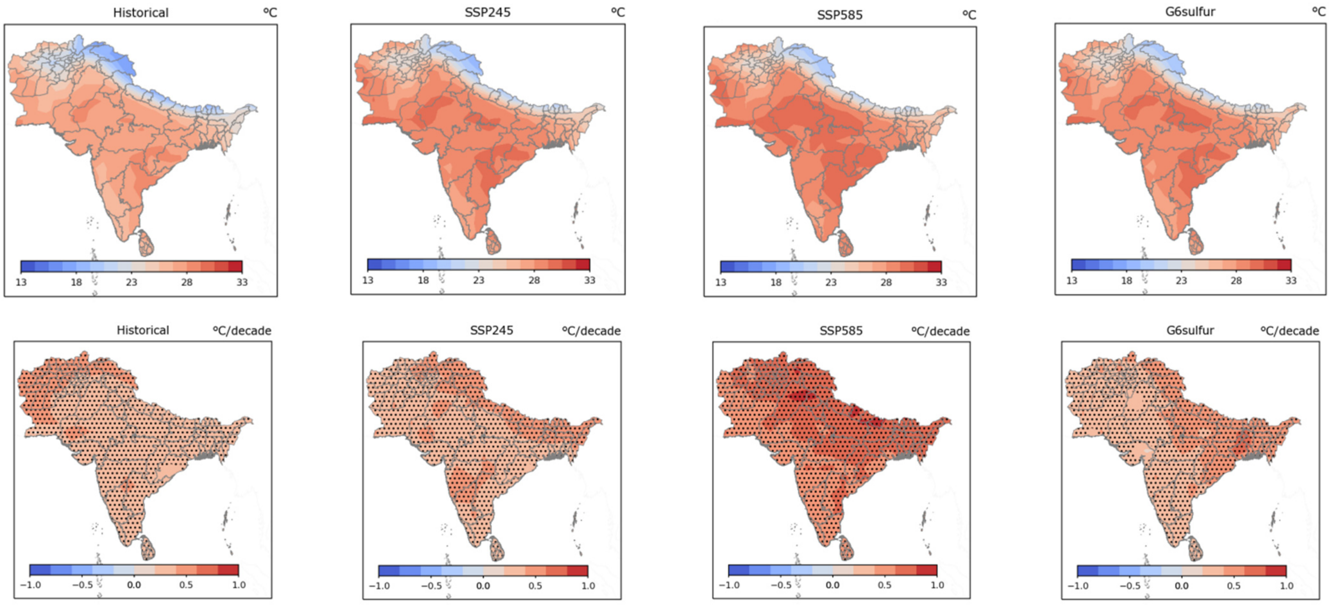

Figure 5. The first row shows mean annual TNx indices under the four scenarios: historical (1985–2014), SSP245 (2030–2059), SSP585 (2030–2059), G6sulfur (2030–2059); the second row shows annual trend of TNx indices under four scenarios: historical, SSP245, SSP585, G6sulfur, where stippling indicates statistically significant trends at a level $p < 0.05$.

Table 6. Trend difference in TNx index among four scenarios (Unit: °C/decade).

Difference / Region	SSP245-Historical	G6sulfur-Historical	G6sulfur-SSP245	G6sulfur-SSP585
Western Afghanistan	−0.3 to −0.1	−0.3 to 0	−0.2 to 0.1	−0.4 to −0.1
Western Deccan Plateau	0 to 0.2	−0.1 to 0.2	−0.3 to −0.1	−0.4 to 0
Thar desert	0.1 to 0.2	−0.2 to 0.1	−0.2 to 0.1	−0.6 to −0.2
The southern slope of the Himalayas	0.1 to 0.2	0.1 to 0.3	−0.1 to 0.3	−0.4 to −0.1

4.5. ID Indices

The ID indices measure the annual number of days with a daily maximum temperature < 0 °C. Under four scenarios (historical, SSP245, SSP585, and G6sulfur), the spatial pattern of the mean annual ID index was predicted to be similar, and the largest values would always occur in Kashmir (Figure 6, first row). Under the historical scenario (1985–2014), the mean annual ID indices in Kashmir would be approximately 120–177 days. Under three future scenarios (2030–2059), the mean annual ID indices would only decrease to 102–164 days in Kashmir. Except for Kashmir, the mean annual ID indices would be about 0–40 days in the whole of South Asia. Comparing the SSP245/G6sulfur scenarios with the historical scenario, the mean annual ID indices would have a significantly larger decline in Kashmir and Afghanistan than in other regions in South Asia (Figure 6, first row). Under the SSP245 scenario (2030–2059), the mean annual ID indices in Kashmir would be predicted to be 12–15 days lower than those during 1985–2014, while the difference in the Deccan Plateau would be just 0–1 days. Under the G6sulfur scenario (2030–2059), changes in the mean annual ID indices were similar to those for the SSP245 scenario. The difference between SSP245 and G6sulfur was predicted to be only 1–3 days. Compared with SSP585 scenario, the G6sulfur scenario would increase the mean annual ID indices in the whole of South Asia by 0–4 days during 2030–2059; a larger increase would occur in northeastern Afghanistan, Kashmir, and the southern slope of the Himalayas.

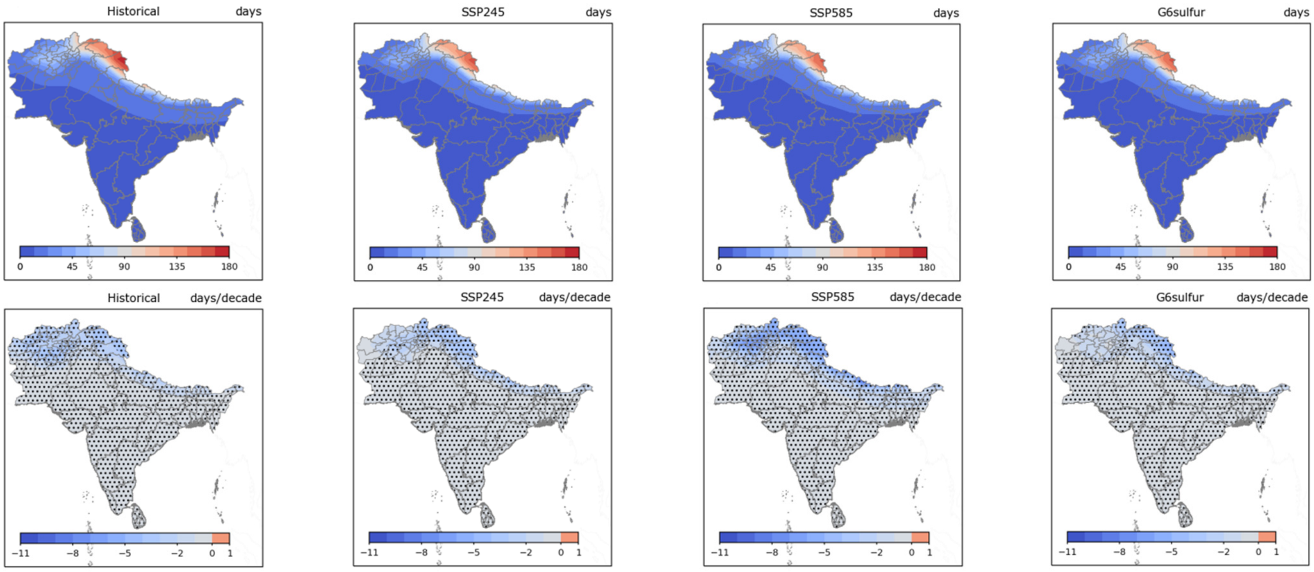

Figure 6. The first row shows mean annual ID indices under the four scenarios: historical (1985–2014), SSP245 (2030–2059), SSP585 (2030–2059), G6sulfur (2030–2059); the second row shows annual trend of ID indices under four scenarios: historical, SSP245, SSP585, G6sulfur, where stippling indicates statistically significant trends at a level $p < 0.05$.

Statistically significant decreasing trends were detected in the whole of South Asia, except for some regions of Afghanistan (Figure 6, second row). Under the historical scenario, the annual ID indices had a decreasing trend (−4 to 0 days/decade) (Figure 6, second row). Under three future scenarios, the annual ID indices were predicted to have a larger decreasing trend (−10 to 0 days/decade). Under all scenarios, a large decreasing trend would only occur in Afghanistan and Kashmir. The significant trend difference in the annual ID indices among four scenarios for representative regions are shown in Table 7.

Table 7. Trend difference in ID index among four scenarios (Unit: °C/decade).

Region \ Difference	SSP245-Historical	G6sulfur-Historical	G6sulfur-SSP245	G6sulfur-SSP585
Afghanistan	0 to 3	0 to 3	−1 to 2	0 to 5
Deccan Plateau	−1 to 0	−1 to 0	−1 to 1	0 to 1
The southern slope of the Himalayas	−1 to 1	−1 to 1	−1 to 3	0 to 5
Kashmir	−1 to 1	−3 to 1	−2 to 1	0 to 4

4.6. CSDI Indices

The CDSI indices measure the annual count of days occurring during at least six consecutive days when the daily minimum temperature is lower than the 10th percentile threshold. Under four scenarios, the mean annual CSDI indices in the Ganges River Plain and interior Deccan Plateau would be much larger than those in other regions in South Asia. Under the historical scenario (1985–2014), the mean annual CSDI indices in the Ganges Plain would be approximately 6–10 days (Figure 7, first row). Under three future scenarios, the mean annual CSDI indices during 2030–2059 would quickly reduce to 0–2 days. Comparing SSP245/G6sulfur scenarios with the historical scenario, the mean annual CSDI indices would have a larger reduction (8–9 days) in the Marva plateau and eastern Deccan Plateau than those in other regions (5–7 days). At the same time, the difference among the SSP245/SSP585 and G6sulfur scenarios was slight (−1 to 1 day).

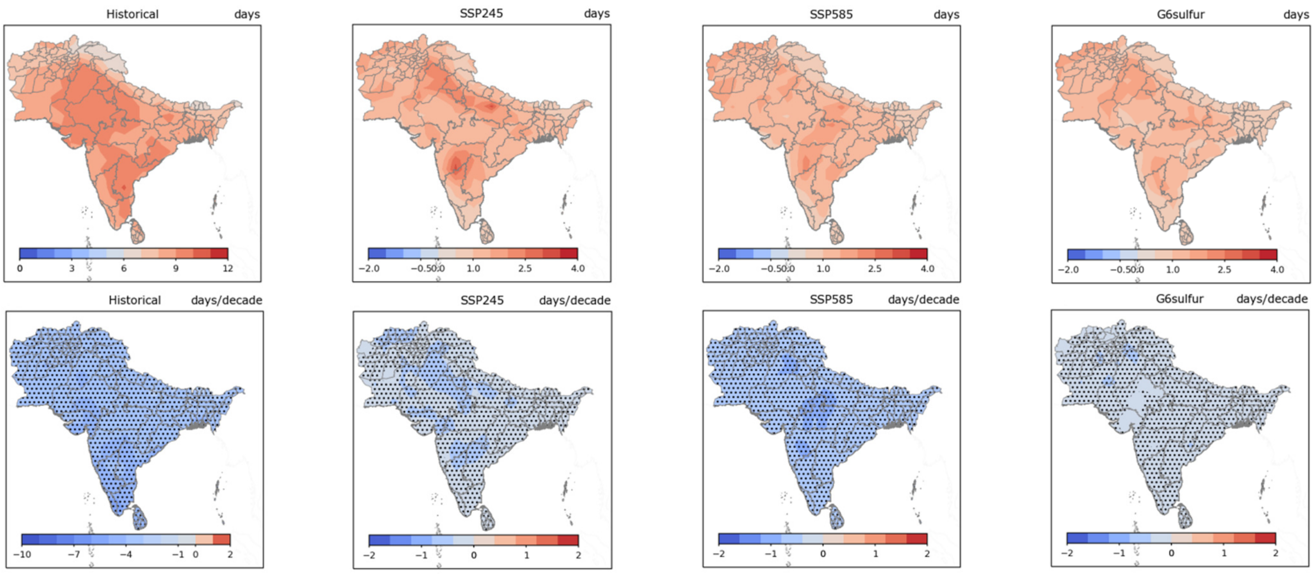

Figure 7. The first row shows mean annual CSDI indices under the four scenarios: historical (1985–2014), SSP245 (2030–2059), SSP585 (2030–2059), G6sulfur (2030–2059); the second row shows annual trend of CSDI indices under four scenarios: historical, SSP245, SSP585, G6sulfur, where stippling indicates statistically significant trends at a level $p < 0.05$.

Under all scenarios, the statistically significant decreasing trends in the CSDI indices were detected in most of South Asia. Under the historical scenario, the decreasing trend was about from −5 to −2 days/decade. Under three future scenarios, the decreasing trend was about from −1 to 0 days/decade (Figure 7, second row). The significant trend difference in the annual CSDI indices among four scenarios for representative regions are shown in Table 8.

Table 8. Trend difference in CSDI index among four scenarios (Unit: days/decade).

Difference / Region	SSP245-Historical	G6sulfur-Historical	G6sulfur-SSP245	G6sulfur-SSP585
Southern Afghanista	2 to 4	2 to 4	−1 to 1	0 to 1
Southern Deccan Plateau	4 to 5	3 to 5	0 to 1	0 to 1
Thar desert	2 to 4	2 to 4	−1 to 1	0 to 1
Middle Deccan Plateau	2 to 4	3 to 4	0 to 1	0 to 1

4.7. TNn Indices

The TNn indices measure the annual minimum value of the daily minimum temperature. Their spatial distribution was similar under all four scenarios (Figure 8, first row). The maximal value appeared in the southern end of South Asia and the minimal value appeared in Kashmir and northern Afghanistan. Under the historical scenario (1985–2014), the mean annual TNn indices in the Deccan Plateau were 5.1–24.1 °C, while under three future scenarios (2030–2059), the mean annual TNn indices in the Deccan Plateau would only reach 6.4–24.4 °C. Comparing the SSP245/G6sulfur scenarios with the historical scenario, the largest difference in the mean annual TNn indices was predicted to appear in the Hindu Kush mountains of northern Afghanistan, Kashmir, and the southern slope of the Himalayas (Figure 8, first row). Under the SSP245 scenario (2030–2059), the mean annual TNn indices in the Hindu Kush mountains of northern Afghanistan, Kashmir, and the southern slope of the Himalayas would be predicted to be 2.7–4.3 °C higher than those during 1985–2014, while the mean annual TNn indices in the Deccan Plateau would be only 0.1–1.6 °C higher. Under the G6sulfur scenario (2030–2059), the mean annual TNn indices in northern Afghanistan, Kashmir, and the southern slope of the Himalayas would be 2.3–5.4 °C higher than those during 1985–2014, while those indices in the Deccan Plateau would be only 0.2–2.1 °C higher. Compared with the SSP245 scenario, the G6sulfur scenario would increase the mean annual TNn indices by 0.1–1.4 °C in almost the whole of South Asia, but in the Ganges River Plain, the mean annual TNn indices would decrease by 0.4–0.9 °C. Compared with the SSP585 scenario, the G6sulfur scenario would decrease the mean annual TNn indices in the Indus-Ganges River Plain by 0.4–1.9 °C, and increase the mean annual TNn indices in the Deccan Plateau by 0.2–0.8 °C.

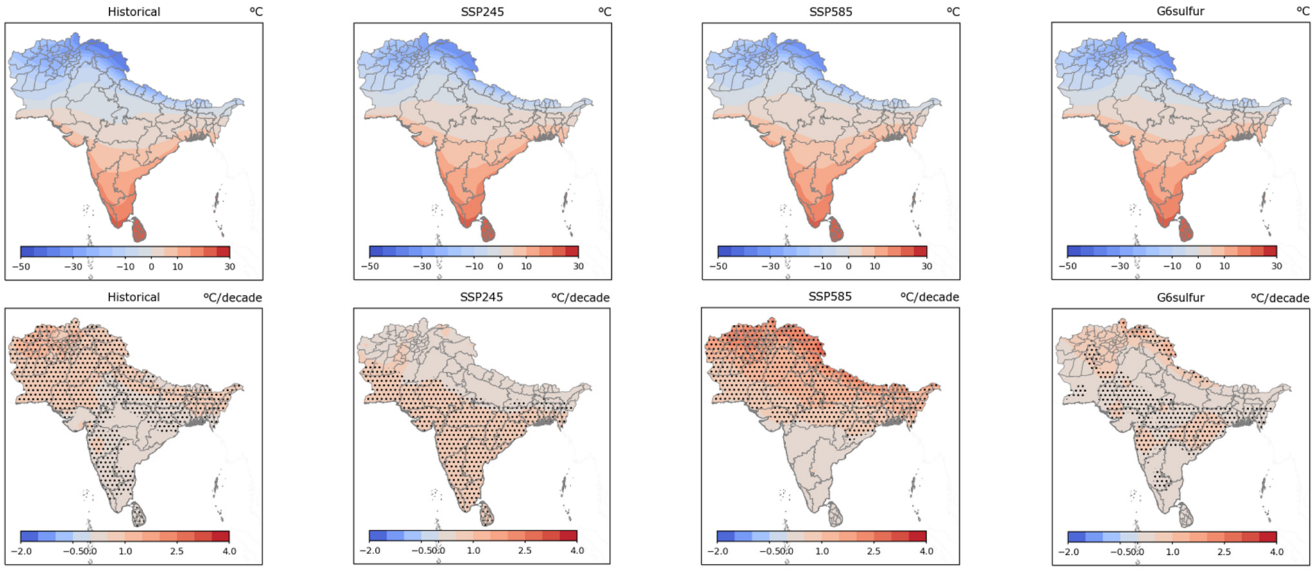

Figure 8. The first row shows mean annual TNn indices under the four scenarios: historical (1985–2014), SSP245 (2030–2059), SSP585 (2030–2059), G6sulfur (2030–2059); the second row shows annual trend of TNn indices under four scenarios: historical, SSP245, SSP585, G6sulfur, where stippling indicates statistically significant trends at a level $p < 0.05$.

Under the historical scenario, the annual TNn indices in South Asia would experience a statistically significant increasing trend (0.1–1.5 °C/decade) (Figure 8, second row). Under the SSP245 scenario, the annual TNn indices in middle and south regions of South Asia would experience a statistically significant increasing trend (0.4–0.9 °C/decade). Under the SSP585 scenario, the annual TNn indices in northern regions of South Asia would experience a statistically significant larger increasing trend (0.5–3.1 °C/decade). Under the G6sulfur scenario, except for the Ganges River Plain and the southern part of the Deccan Plateau, the annual TNn index would experience a statistically significant increasing trend (0.1–0.6 °C/decade). The significant trend difference in the annual TNn indices among four scenarios for representative regions are shown in Table 9.

Table 9. Trend difference in TNn index among four scenarios (Unit: °C/decade).

Region \ Difference	SSP245-Historical	G6sulfur-Historical	G6sulfur-SSP245	G6sulfur-SSP585
Afghanistan	−0.9 to −0.2	−0.6 to −0.1	−0.1 to 0.6	−1.8 to −0.5
The southern slope of the Himalayas	−0.7 to −0.1	−0.5 to 0.6	−0.3 to 1.2	−1.4 to −0.1
Western Deccan Plateau	0.1 to 0.6	−0.2 to 0.2	−0.4 to −0.1	0 to 0.4
Marva Plateau	0 to 0.5	−0.2 to 0.3	−0.1 to 0	0.1 to 0.3

4.8. TXn Indices

The TXn indices measure the annual maximal value of the daily minimum temperature. Similar to the TNn indices, the spatial distribution of the mean annual TXn indices was also similar under all four scenarios (Figure 9, first row). The maximal value appeared in the southern end of the Indian Peninsula and the minimal value appeared in Kashmir and northern Afghanistan. Under the historical scenario (1985–2014), the mean annual TXn indices in the Indian Peninsula would be approximately 19.4–25.8 °C (Figure 9, first row). Compared with the historical scenario, under three future scenarios (2030–2059), the mean annual TXn indices would rise to 20.7–27.1 °C in the Indian Peninsula. However, due to a rapid increase in altitude, the mean annual TXn indices in Kashmir would be from −21.1 to −11.8 °C. Comparing the SSP245/G6sulfur scenarios with the historical scenario, the largest warming was predicted to occur in the Hindu Kush mountain range in northern Afghanistan. Under the SSP245 scenario (2030–2059), the mean annual TXn indices in the Hindu Kush mountain range would have rise by 1.1–2.2 °C, while those indices in the Deccan Plateau would only rise by 0.8–1.5 °C. Under the G6sulfur scenario (2030–2059), the mean annual TXn indices would have rise by 1.5–2.6 °C in the Hindu Kush and rise by 0.9–1.8 °C in the Deccan Plateau compared with those during 1985–2014. Compared with the SSP245 scenario, the G6sulfur scenario would lead to a larger rise in the mean annual TXn indices by 0.1–1.1 °C in northern regions of South Asia. However, the warming of the mean annual TXn indices in the Deccan Plateau would be mitigated by 0–0.1 °C. Compared with SSP585 scenario, the G6sulfur scenario would lead to a rise in mean annual TXn indices in the northern Deccan Plateau and Ganges Delta during 2030–2059 by 0.2–0.6 °C, and a decline in the mean annual TXn indices in the northern Indus River Plain and upper Ganges River Plain by 0.3–0.6 °C.

Under the historical scenario, the annual TXn indices in the Deccan Plateau, Afghanistan, and the southern slope of the Himalayas had a statistically significant increasing trend (0.1–1.4 °C/decade) (Figure 9, second row). Under the SSP245 scenario, the annual TXn indices in most of South Asia would have a statistically significant increasing trend (0.2–0.9 °C/decade). Under the SSP585 scenario, except for western Afghanistan and the lower Indus River Plain, the annual TXn indices would have a statistically significant increasing trend (0.3–1.1 °C/decade). Under the G6sulfur scenario, the annual TXn indices in the Deccan Plateau and the southern slope of the Himalayas would have a statistically significant increasing trend (0.2–1.1 °C/decade). The significant trend difference in the annual TXn indices among four scenarios for representative regions are showed in Table 10.

Table 10. Trend difference in TXn index among four scenarios (Unit: °C/decade).

Region \ Difference	SSP245-Historical	G6sulfur-Historical	G6sulfur-SSP245	G6sulfur-SSP585
Eastern Afghanistan	−0.8 to 0	−0.7 to 0	−0.5 to 0	−0.7 to −0.4
Middle Deccan Plateau	−0.3 to 0.3	−0.2 to 0.3	−0.4 to 0.3	−0.3 to −0.1
Thar Desert	0 to 0.4	−0.4 to 0	−0.5 to −0.1	−0.6 to 0
The southern slope of the Himalayas	−0.2 to 0.3	−0.2 to 0.4	−0.4 to 0.2	−0.6 to −0.1

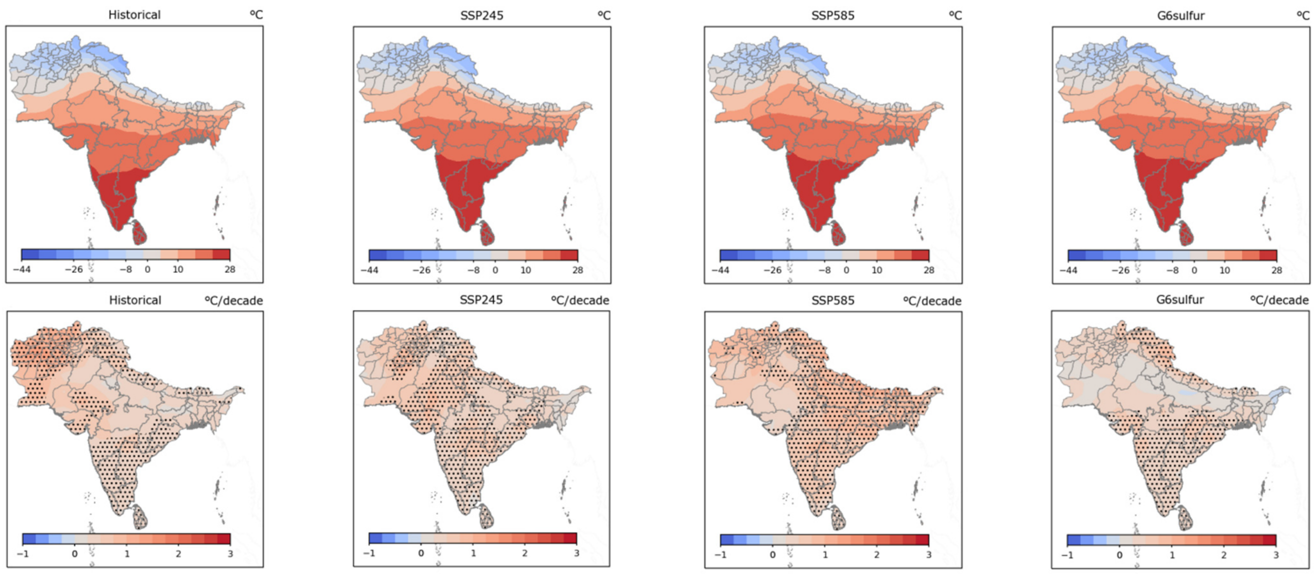

Figure 9. The first row shows mean annual TXn indices under the four scenarios: historical (1985–2014), SSP245 (2030–2059), SSP585 (2030–2059), G6sulfur (2030–2059); the second row shows annual trend of TXn indices under four scenarios: historical, SSP245, SSP585, G6sulfur, where stippling indicates statistically significant trends at a level $p < 0.05$.

4.9. CDD Indices

The CDD indices measure the maximum number of consecutive days when precipitation is <1 mm. Under the historical scenario and three future scenarios, the spatial distribution of the mean annual CDD indices would have little difference. The highest value would appear in the Sistan Basin of southern Afghanistan, and the lowest value would appear on the southern slope of the eastern Himalayas (Figure 10, first row). Under the historical scenario (1985–2014), the mean annual CDD indices in the Sistan Basin would be 100–154 days. Under three future scenarios (2030–2059), the mean annual CDD indices in the Sistan Basin would rise further to 103–168 days. Due to the fact that South Asian monsoons are blocked by the Himalayas, the mean annual CDD indices in the southern slope of the Himalayas would be only 36–73 days. Under the SSP245 scenario, during 2030–2059, the mean annual CDD indices in western Afghanistan and the Lower Indus River Plain would be predicted to be 6–17 days higher than those during 1985–2014, while those in the Deccan Plateau and the southern slope of the Himalayas would be predicted to be 1–6 days lower. Under the G6sulfur scenario, the mean annual CDD indices in western Afghanistan would be predicted to be 10–19 days higher than those during 1985–2014, while these indices in the southern slope of the Himalayas would be predicted to be 1–12 days lower than those during 1985–2014. Compared with the SSP245 scenario, except for the Ganges River Plain, the implementation of SAI climate engineering would increase the mean annual CDD indices in almost the whole of South Asia by 1–10 days during 2030–2059. Especially, an increase of 5–10 days would occur in western Afghanistan. Compared with the SSP585 scenario, the implementation of SAI climate engineering would increase the mean annual CDD indices in most of South Asia by 1–8 days from 2030 to 2059, except for the southern slope of the Himalayas. Especially, an increase of 5–8 days in the Sistan Basin and an increase of 1–5 days in the Deccan Plateau, and a decrease of 1–6 days on the southern slope of the Himalayas would be expected.

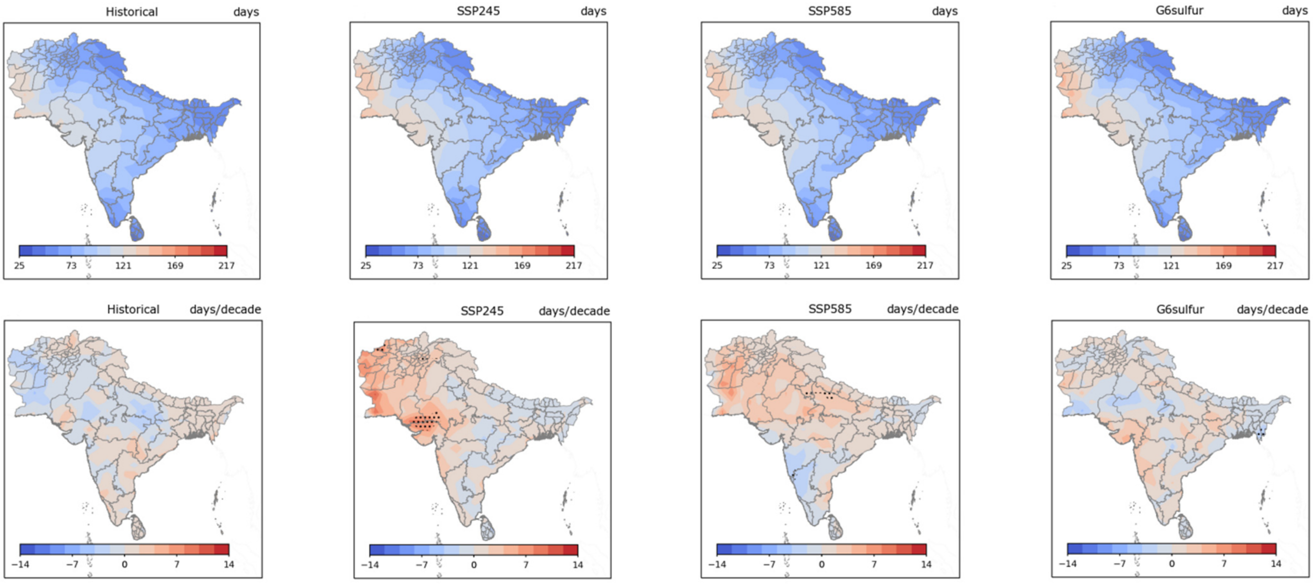

Figure 10. The first row shows mean annual CDD indices under the four scenarios: historical (1985–2014), SSP245 (2030–2059), SSP585 (2030–2059), G6sulfur (2030–2059); the second row shows annual trend of CDD indices under four scenarios: historical, SSP245, SSP585, G6sulfur, where stippling indicates statistically significant trends at a level $p < 0.05$.

Under the historical scenario and three future scenarios, the annual trend of the CDD indices could not pass the statistical significance test at the level of $p < 0.05$ in almost all of South Asia (Figure 10, second row). Under the historical scenario, the annual trend of the CDD indices had a slight increasing trend in the Deccan Plateau and a slight decreasing trend in western Afghanistan and the Indus River Plain (Figure 10, second row). Under the SSP245 scenario, only the annual trend of the CDD indices in the southern Marva Plateau would be statistically significant (2–11 days/decade). Under the SSP585 scenario, the annual CDD indices would have a slight decreasing trend (−2 to −4 days/decade) in most of the Deccan Plateau and a slight increasing trend (2–4 days/decade) in Afghanistan and the Indus-Ganges River Plain. Under the G6sulfur scenario, the annual CDD indices would have a slight increasing trend in the Deccan Plateau and a slight decreasing trend in the southern Indus River Plain and Ganges Delta. The significant trend difference in the annual CDD indices among four scenarios for representative regions are shown in Table 11.

Table 11. Trend difference in CDD index among four scenarios (Unit: days/decade).

Difference / Region	SSP245-Historical	G6sulfur-Historical	G6sulfur-SSP245	G6sulfur-SSP585
Western Afghanistan	1 to 4	1 to 3	−4 to 0	−5 to 1
Ganges Delta	−3 to −1	−4 to 0	−2 to 2	−4 to 1
Western Deccan Plateau	−1 to 7	−2 to 5	−4 to 3	4 to 7
Southwestern Indus River Plain	3 to 6	−4 to 4	−8 to −1	−7 to −1

4.10. CWD Indices

The CWD indices measure the maximum number of consecutive days when precipitation is ≥1 mm. Under four scenarios, affected by southwest monsoons, the largest value of the mean annual CWD indices would appear in the western Deccan Plateau (up to 60 days). The minimal value would appear in the Thar desert, Afghanistan, and Kashmir (about 10–14 days) (Figure 11, first row). Compared with the historical scenario, the mean annual

CWD indices under the SSP245 scenario would be predicted to be 2–4 days higher in the eastern Deccan Plateau, 1–2 days higher in the Thar desert, Indus river plain, Afghanistan, and Kashmir, and 1–2 days lower in the western Ghats and near the Ganges Delta. This is similar to the difference between the G6sulfur and historical scenarios. The mean annual CWD indices under the G6sulfur scenario would be predicted to be 1–2 days less than those in SSP245 scenario in most regions in South Asia, but 2–3 days larger in the western Ghats. Compared with the SSP585 scenario, the G6sulfur scenario would decrease the mean annual CWD indices in most South Asian regions by 0–2 days, and the largest decrease would appear in the south end of the Deccan Plateau.

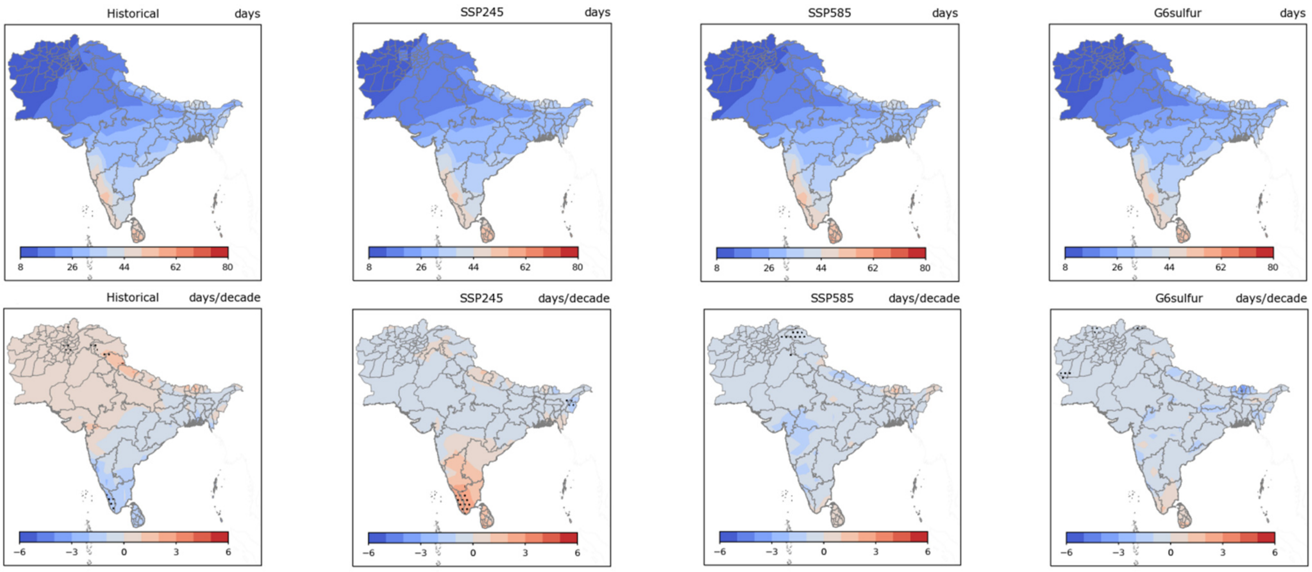

Figure 11. The first row shows mean annual CWD indices under the four scenarios: historical (1985–2014), SSP245 (2030–2059), SSP585 (2030–2059), G6sulfur (2030–2059); the second row shows annual trend of CWD indices under four scenarios: historical, SSP245, SSP585, G6sulfur, where stippling indicates statistically significant trends at a level $p < 0.05$.

Under the historical scenario and three future scenarios, the annual trend of the CWD indices could not pass the statistical significance test at the level $p < 0.05$ in almost all South Asian regions (Figure 11, second row). Under the historical scenario, the annual CWD indices would have a slight decreasing trend in southeast regions and a slight increasing trend in northwest regions of South Asia. Under the SSP245 scenario, the annual CWD indices would show a statistically significant increasing trend (2–4 days/decade) only in the southern part of the Deccan Plateau. Under the SSP585 and G6sulfur scenarios, the annual trend of the CWD index in most of South Asia would be slight. The significant trend difference in the annual CWD indices among four scenarios for representative regions are shown in Table 12.

Table 12. Trend difference in CWD index among four scenarios (Unit: days/decade).

Region \ Difference	SSP245-Historical	G6sulfur-Historical	G6sulfur-SSP245	G6sulfur-SSP585
Afghanistan	−1 to 0	−1 to 0	−1 to 1	−1 to 1
Southern Deccan Plateau	2 to 6	1 to 4	−4 to 0	0 to 2
Southern Indus River Plain	−1 to 0	−1 to 0	−1 to 1	0 to 1
The southern slope of the Himalayas	−3 to 0	−5 to 1	−4 to 1	−5 to 2

4.11. RX1day Indices

The RX1day indices measure the maximum daily precipitation. Under all four scenarios, the largest value of the RX1day indices would appear in the Ganges Delta and the smallest value would appear in Afghanistan and the Indus River Plain (Figure 12, first row). Under the SSP245 scenario, the mean annual RX1day indices would be 4.3–13.1 mm higher in western coastal regions and about 1 mm lower in Afghanistan than those from 1985 to 2014. Under the G6sulfur scenario, the mean annual RX1day indices would be 2.3–10.2 mm higher in the Gangetic River Plain and 1.2–10.1 mm higher in the southern Deccan Plateau than those from 1985 to 2014. Compared with the SSP245 scenario, the G6sulfur scenario would decrease the mean annual RX1day indices in western coastal regions by 3.1–10.4 mm and increase the indices in other regions in South Asia by 0.1–7.4 mm. Compared with the SSP585 scenario, the G6sulfur scenario would increase the mean annual RX1day indices in the southern Deccan Plateau, Marva Plateau, and upper Indus River Plain by 0.1–4.7 mm, and decrease those indices in the Ganges Delta by at most 5 mm.

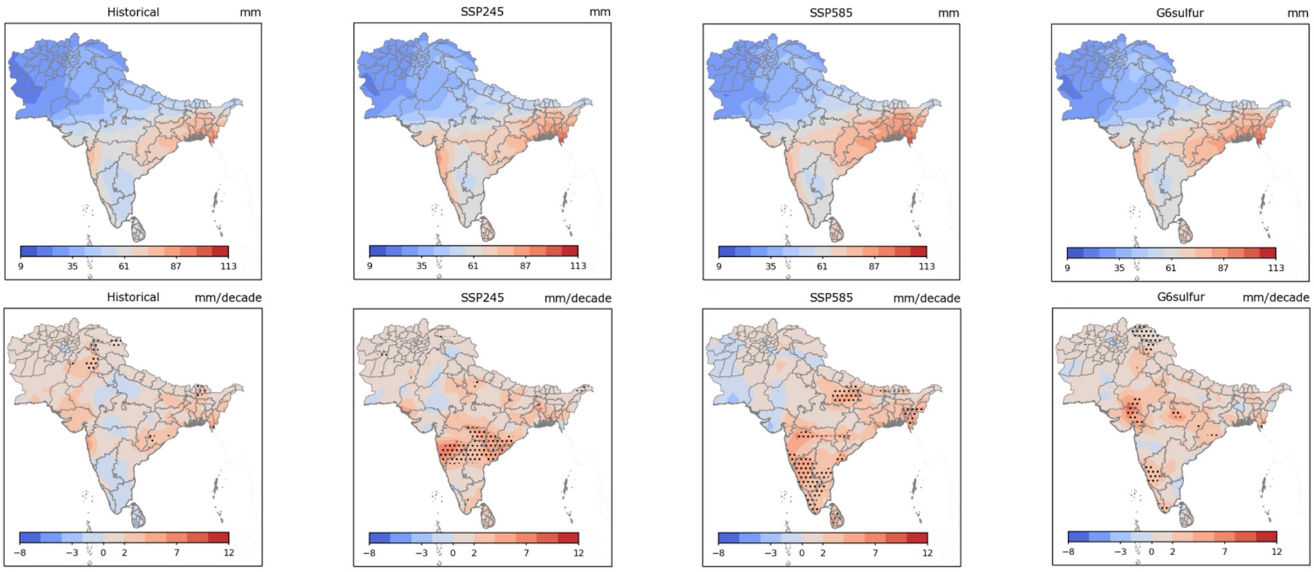

Figure 12. The first row shows mean annual RX1day indices under the four scenarios: historical (1985–2014), SSP245 (2030–2059), SSP585 (2030–2059), G6sulfur (2030–2059); the second row shows annual trend of RX1day indices under four scenarios: historical, SSP245, SSP585, G6sulfur, where stippling indicates statistically significant trends at a level $p < 0.05$.

The annual trends of the RX1day indices in most of South Asia would not be statistically significant (Figure 12, second row). The limited regions with statistically significant trends include: 3.3–7.4 mm/decade in the northern Deccan Plateau under the SSP245 scenario; 2.3–7.1 mm/decade in the southern Deccan Plateau and middle Ganges River Plain under the SSP585 scenario; 4.3–8.5 mm/decade in the Thar desert under the G6sulfur scenario. The significant trend differences in the annual RX1day indices among four scenarios for representative regions are shown in Table 13.

Table 13. Trend difference in RX1day index among four scenarios (Unit: mm/decade).

Difference / Region	SSP245-Historical	G6sulfur-Historical	G6sulfur-SSP245	G6sulfur-SSP585
Ganges Delta	−2.6 to 2.5	−4.3 to 2.1	−6.6 to 3.4	−5.4 to 2.3
Middle Deccan Plateau	2.1 to 7.3	−6.9 to 6.4	−5.8 to −0.3	−5.3 to −0.2
Indus River Plain	−4.6 to 1.2	−2.2 to 1.5	−2.6 to 4.5	−1.6 to 5.2
Marva Plateau	−2.1 to 1.1	−2.3 to 6.4	3.3 to 8.1	2.4 to 7.9

We compared the mean summer and annual RX1day indices (Figures 12 and 13). Due to a monsoon climate, the summer season had a significant share of the annual RX1day indices. Under the historical scenario, the mean summer RX1day indices in the Ganges Delta would account for 83.8–90% of the mean annual RX1day indices. Under three future scenarios, the mean summer RX1day indices in the Ganges Delta would account for 85–87% of the mean annual RX1day indices. We compared, further, the trend differences in the annual and summer RX1day indices (Figures 12 and 13). Comparing the G6sulfur scenario with the historical scenario, the summer RX1day indices in the southern Deccan Plateau and Marva Plateau would have a significant increasing trend difference, about 1.4 mm/decade slower than the trend difference in the annual RX1day indices. Comparing the G6sulfur scenario with the SSP245 scenario, the summer RX1day indices in the north Deccan Plateau would have an additional decreasing trend (−2.9 to −0.9 mm/decade), while the annual RX1day indices would have an additional more quickly decreasing trend (−5.8 to −3.2 mm/decade).

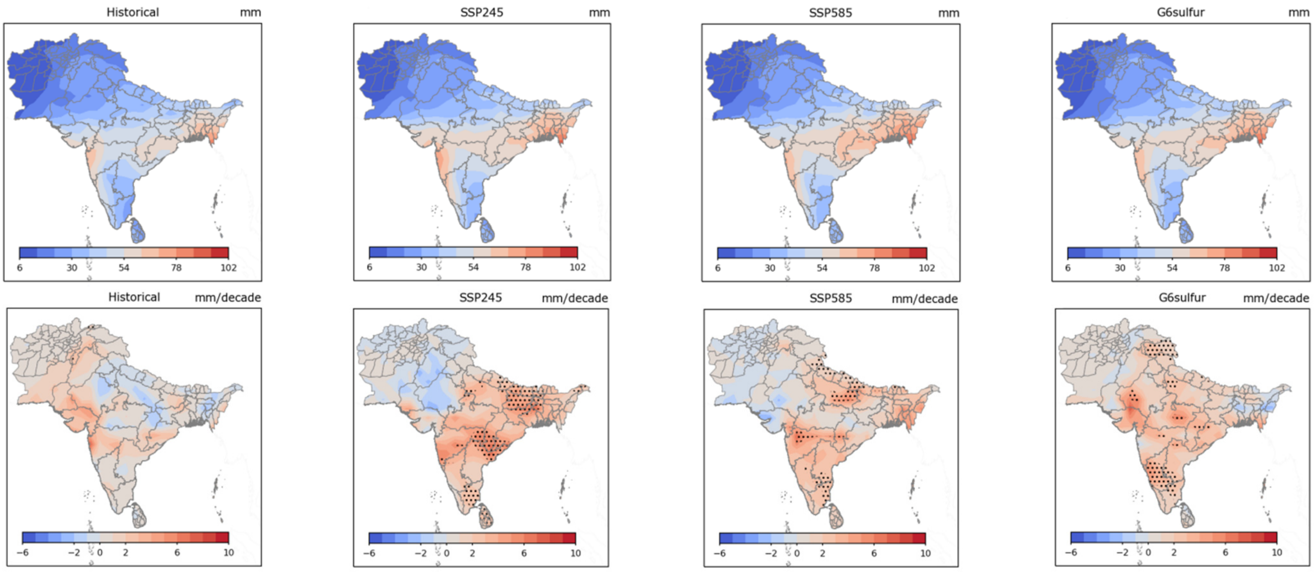

Figure 13. The first row shows mean summer RX1day indices under the four scenarios: historical (1985–2014), SSP245 (2030–2059), SSP585 (2030–2059), G6sulfur (2030–2059); the second row shows Trend of summer RX1day indices under four scenarios: historical, SSP245, SSP585, G6sulfur, where stippling indicates statistically significant trends at a level $p < 0.05$.

We examined the link between the annual RX1day indices and the annual precipitation (Figure 14). Under all four scenarios, the annual RX1day indices and the annual precipitation in South Asia were always positively correlated, especially under the G6sulfur scenario, the correlation in the southwestern Indus River Plain and the Marva Plateau are strong (0.61–0.68), while the correlation in the rest of South Asia is weak.

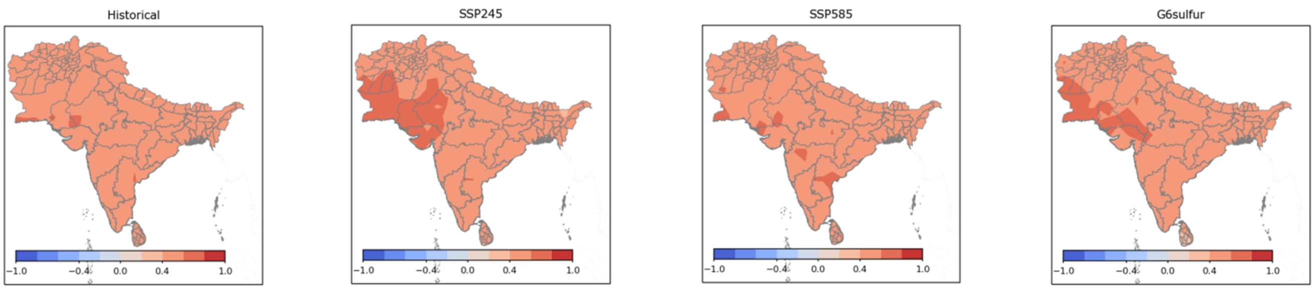

Figure 14. Pearson correlation coefficients between annual RX1day indices and annual precipitation under four scenarios: historical (1985–2014), SSP245 (2030–2059), SSP585 (2030–2059), G6sulfur (2030–2059).

4.12. RX5day Indices

The RX5day indices measure the maximum of consecutive five-day precipitation amounts. Under all four scenarios, the highest values of the mean annual RX5day indices (>250 mm) would appear in the Ganges Delta and western Ghats while the lowest values (<50 mm) would appear in the Sistan Basin of south Afghanistan (Figure 15, first row). Compared with the historical scenario (1985–2014), the mean annual RX5day indices under the SSP245 scenario would be predicted to be 12.1–31.2 mm higher in the western Ghats, 8.2–19.8 mm higher on the southern slope of the Himalayas, and 2.7–11.6 mm lower in the eastern Ghats, and the mean annual RX5day indices under G6sulfur scenario would be predicted to be 8.1–26.5 mm higher in the Lower Ganges River Plain and 2.3–10.7 mm lower in the western/eastern Ghats.

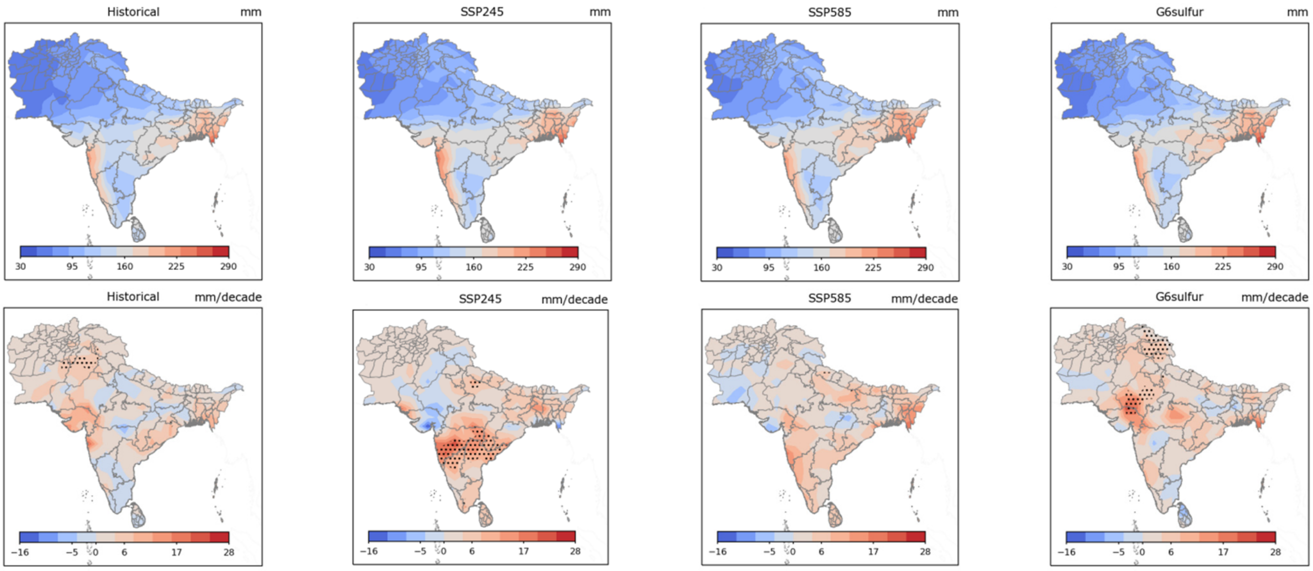

Figure 15. The first row shows the mean annual RX5day indices under the four scenarios: historical (1985–2014), SSP245 (2030–2059), SSP585 (2030–2059), G6sulfur (2030–2059); the second row shows annual trend of RX5day indices under four scenarios: historical, SSP245, SSP585, G6sulfur, where stippling indicates statistically significant trends at a level $p < 0.05$.

Compared with the SSP245 scenario, except for coastal regions adjacent to the Arabian Sea, the G6sulfur scenario would increase the mean annual RX5day indices by 0.1–20.9 mm in the whole of South Asia; especially, by 8.5–20.9 mm in the middle of the Ganges River Plain and 0.1–6.1 mm in the northern Indus River Plain. At the same time, the mean annual RX5day indices would decrease by 0.8–28.3 mm in coastal regions adjacent to the Arabian Sea. Compared with the SSP585 scenario, the G6sulfur scenario would bring a 0.2–11.9 mm increase in the mean annual RX5day indices in most regions in the Indian peninsula and a 2.1–26.1 mm decrease in the southern Indus River Plain.

The annual trends of the RX5day indices under four scenarios are statistically insignificant in most regions of South Asia (Figure 15, second row). Limited regions with statistically significant increasing trends of annual RX5day indices include a 7.3–23.8 mm/decade trend in the northern Deccan Plateau under the SSP245 scenario, and a 1.1–22.4 mm/decade trend in the Thar desert and Kashmir under the G6sulfur scenario. The significant trend differences in the annual RX5day indices among four scenarios for representative regions are shown in Table 14.

Table 14. Trend difference in RX5day index among four scenarios (Unit: mm/decade).

Region \ Difference	SSP245-Historical	G6sulfur-Historical	G6sulfur-SSP245	G6sulfur-SSP585
Ganges Delta	−10.9 to 17.8	−7.1 to 8.9	−20.1 to 29.8	−19.4 to 4.2
Middle Deccan Plateau	5.3 to 21.6	−10.4 to 17.4	−28.6 to 7.6	−11.3 to 16.7
Indus river plain	−11.9 to 2.1	−7.2 to 3.5	−7.2 to 13.4	−3.1 to 9.4
Marwa Plateau	−16.9 to −4.3	−13.4 to 17.4	1.2 to 33.8	0.8 to 16.7

5. Conclusions

Due to global climate change, South Asia is facing dual pressures of the obligation of carbon emissions reduction globally and the demand for a better life for huge populations. SAI climate engineering seemingly provides a solution to this dilemma. As the most important simulation of SAI climate engineering, the G6sulfur experiment is designed to inject SO2 into the stratosphere starting from 2020 in order to reduce the high radiative forcing (SSP585) to medium radiative forcing (SSP245) [7]. Although all simulations indicated that SAI climate engineering would be expected to reduce the increase in mean surface temperature to the pre-industrial level, the correlation coefficient between climate extreme indices and the mean climate is only about 0.5, leading to the conclusion that to control the increase in mean temperature/precipitation by SAI climate engineering does not mean controlling the change in climate extremes well. Therefore, we analyzed the evolution of extreme climates under four scenarios (historical, SSP245, SSP585, and G6sulfur) through 12 widely-used extreme indices in detail. These indices can reflect difference aspects of climate extremes, from warm temperature extremes and cold temperature extremes to precipitation/drought extremes. Five indices (TXx, TNx, TXn, TNn, Rx1day) reveal extreme values in temperature and precipitation, while seven indices (SU, WSDI, ID, CSDI, CDD, CWD, Rx5day) reveal the duration of temperature/precipitation/drought extremes. At the same time, different climatic conditions are spread over wide and diverse geographic regions of South Asia, including arid regions, low-lying coastal regions, alluvial plain regions, tropical regions, and mountainous regions, leading to diverse responses of the different climate extreme indices to the implementation of SAI climate engineering.

Our analysis of 12 extreme indices revealed that the intensities and frequency of extreme climates under G6sulfur scenario would be significantly higher than those under historical scenarios due to the fact that the radiative forcing level in the G6sulfur experiment is only reduced compared to the SSP245 scenario through the implementation of SAI climate engineering, and these would be much higher than those under the historical scenario. Since different climatic conditions are spread over wide and diverse geographic regions of South Asia, we selected three representative terrains (plateau region, plain region, mountain region) in South Asia, covering over 50% of the area of south Asia, and revealed very different impacts of the implementation of SAI climate engineering on climate extremes in these regions under three future scenarios:

- Deccan Plateau: (a) Compared with the SSP245 scenario, the G6sulfur scenario would increase the WSDI indices by 7–15 days, the TNn indices by 0.1–1.4 °C, the CDD indices by 1–10 days, and the RX5day indices by 0.2–11.9 mm, but decrease the SU indices by 1–4 days, the TXn indices by 0–0.1 °C, and the CWD indices by 1–2 days. (b) Compared with the SSP585 scenario, the G6sulfur scenario would increase the TNn indices by 0.2–0.8 °C and the CDD indices by 1–5 days, but decrease the WDSI indices by 12–23 days, the TXx indices by 0.1–0.4 °C, and the CWD indices by 1–2 days.
- Ganges River Plain: (a) Compared with the SSP245 scenario, the G6sulfur scenario would increase the SU indices by 1–3 days and the TXn indices by 0.1–1.1 °C, but decrease the TNn indices by 0.4–0.9 °C and the CWD indices by 1–2 days. (b) Compared with the SSP585 scenario, the G6sulfur scenario would increase the TNx indices by 0–0.2 °C and the CDD indices by 1–8 days, but decrease the SU indices by 1–12 days,

the TXx indices by 0.1–0.4 °C, the TNn indices by 0.4–1.9 °C, and the CWD indices by 1–2 days.

- Kashmir and Himalayas Mountain Ranges: (a) Compared with the SSP245 scenario, the G6sulfur scenario would increase the SU indices by 1–3 days, the WSDI indices by 1–2 days, the TXx indices by 0.2–0.9 °C, the TNx indices by 0.3–0.6 °C, the TXn indices by 0.1–1.1 °C, and the TNn indices by 0.1–1.4 °C, but would decrease the CWD indices by 1–2 days. (b) Compared with the SSP585 scenario, the G6sulfur scenario would increase the RX5day indices by 0.2–11.9 mm and the ID indices by 1–3 days, and decrease the TXx indices by 0.1–0.4 °C, the CDD indices by 1–6 days, and the CWD indices by 1–2 days.

Although all simulations reveal that the implementation of SAI climate engineering would decrease the mean temperature, our study found that significant differences in extreme climates response to three future scenarios: some indices were mitigated considerably, while others may reflect a worse set of circumstances than would be the case without the implementation of SAI climate engineering. Moreover, by comparing summer and annual extreme indices, we reveal that seasonal factors would not play a significant factor in the evolution of these climate extreme indices. It is worth noting that, although the radiative forcing level in the G6sulfur experiment is reduced compared to the SSP245 scenario, the Kashmir and Himalayas Mountain Ranges were predicted to have more extreme warm events under the G6sulfur scenario than under the SSP245 scenario. Since these regions are the source of major rivers in South Asia, such a warming would possibly cause further mountain glacier retraction and result in the frequent occurrence of flood events. In summary, SAI climate engineering is not an effective tool to mitigate future climate extremes in South Asia under a global warming scenario.

Author Contributions: J.W. and Z.Z. are co-first authors. Conceptualization, Z.Z.; Methodology, Z.Z.; Software, J.W.; Formal analysis, Z.Z. and J.W.; Data curation, J.W. and L.C.D.; Writing—original draft, Z.Z. and J.W.; Writing—review & editing, Z.Z. and M.J.C.C.; Visualization, J.W.; Project administration, Z.Z. All authors have read and agreed to the published version of the manuscript.

Funding: The corresponding author was supported by the European Commission Horizon 2020 Framework Program No. 861584 and the Taishan Distinguished Professor Fund No. 20190910.

Institutional Review Board Statement: Not applicable.

Informed Consent Statement: Not applicable.

Data Availability Statement: Not applicable.

Conflicts of Interest: The authors declare no conflict of interest.

References

1. Clark, C.P.; Cazenave, A.; Gregory, J.; Unnikrishnan, A. *Climate Change 2013: The Physical Science Basis: Contribution of Working Group I to the Fifth Assessment Report of the Intergovernmental Panel on Climate Change*; Cambridge University Press: Cambridge, UK, 2013.
2. Zhu, Y.; Zhang, Z.; Crabbe, M. Extreme climate response to marine cloud brightening in the arid Sahara-Sahel-Arabian Peninsula zone. *Int. J. Clim. Change Strat. Manag.* **2021**, *13*, 250–265. [CrossRef]
3. Shepherd, J.G. *Geoengineering the Climate: Science, Governance and Uncertainty*; Royal Society: London, UK, 2009.
4. Jones, A.; Haywood, J.M.; Jones, A.C.; Tilmes, S.; Kravitz, B.; Robock, A. North Atlantic Oscillation response in GeoMIP experiments G6solar and G6sulfur: Why detailed modelling is needed for understanding regional implications of solar radiation management. *Atmos. Chem. Phys.* **2021**, *21*, 1287–1304. [CrossRef]
5. MacMartin, D.G.; Kravitz, B.; Tilmes, S.; Richter, J.H.; Mills, M.J.; Lamarque, J.; Tribbia, J.J.; Vitt, F. The Climate response to Stratospheric Aerosol Geoengineering can be tailored using multiple injection locations. *J. Geophys. Res. Atmos.* **2017**, *122*, 574–590. [CrossRef]
6. Duffey, A.; Irvine, P.; Tsamados, M.; Stroeve, J. Solar Geoengineering in the Polar Regions: A Review. *Earth's Future* **2023**, *11*, e2023EF003679. [CrossRef]
7. Jones, A.; Haywood, J.M.; Scaife, A.A.; Boucher, O.; Henry, M.; Kravitz, B.; Lurton, T.; Nabat, P.; Niemeier, U.; Seferian, R.; et al. The impact of stratospheric aerosol intervention on the North Atlantic and Quasi-Biennial Oscillations in the Geoengineering Model Intercomparison Project (GeoMIP) G6sulfur experiment. *Atmos. Chem. Phys.* **2022**, *22*, 2999–3016. [CrossRef]

8. Kravitz, B.; Robock, A.; Tilmes, S.; Boucher, O.; English, J.M.; Irvine, P.J.; Jones, A.; Lawrence, M.G.; MacCracken, M.; Muri, H.; et al. The Geoengineering model intercomparison project phase 6 (GeoMIP6): Simulation design and preliminary results. *Geosci. Model Dev.* **2015**, *8*, 4697–4736. [CrossRef]
9. Diamond, M.S.; Wanser, K.; Boucher, O. "Cooling credits" are not a viable climate solution. *Clim. Change* **2023**, *176*, 96. [CrossRef]
10. Tilmes, S.; Visioni, D.; Jones, A.; Haywood, J.; Séférian, R.; Nabat, P.; Boucher, O.; Bednarz, E.M.; Niemeier, U. Stratospheric ozone response to sulfate aerosol and solar dimming climate interventions based on the G6 Geoengineering Model Intercomparison Project (GeoMIP) simulations. *Atmos. Chem. Phys.* **2022**, *22*, 4557–4579. [CrossRef]
11. Tang, W.; Tilmes, S.; David, M.L.; Li, F.; He, C.; Louisa, K.E.; Rebecca, R.B.; Xia, L. Impact of solar geoengineering on wildfires in the 21st century in CESM2/WACCM6. *Atmos. Chem. Phys.* **2023**, *23*, 5467–5486. [CrossRef]
12. Liu, Z.; Lang, X.; Miao, J.; Jiang, D. Impact of Stratospheric Aerosol Injection on the East Asian Winter Monsoon. *Geophys. Res. Lett.* **2023**, *50*, e2022GL102109. [CrossRef]
13. Liang, J.; Haywood, J. Future changes in atmospheric rivers over East Asia under stratospheric aerosol intervention. *Atmos. Chem. Phys.* **2023**, *23*, 1687–1703. [CrossRef]
14. Katzenberger, A.; Schewe, J.; Pongratz, J.; Levermann, A. Robust increase of Indian monsoon rainfall and its variability under future warming in CMIP6 models. *Earth Syst. Dyn.* **2021**, *12*, 367–386. [CrossRef]
15. Huang, J.; Sanjit, K.M.; Zhai, J.; Thomas, F.; Wang, Y.; Su, B.; Wang, G.; Gao, M.; Jiang, S.; Tao, H.; et al. Intensity-area-duration-based drought analysis under 1.5 °C–4.0 °C warming using CMIP6 over a climate hotspot in South Asia. *J. Clean. Prod.* **2022**, *345*, 131106. [CrossRef]
16. Pachauri, R.K.; Allen, M.R.; Barros, V.R.; Broome, J.; Cramer, W.; Christ, R.; Church, J.A.; Clarke, L.; Dahe, Q.; Dasgupta, P.; et al. *Climate Change 2014: Synthesis Report. Contribution of Working Groups I, II and III to the Fifth Assessment Report of the Intergovernmental Panel on Climate Change*; IPCC: Geneva, Switzerland, 2014.
17. O'Neill, B.C.; Tebaldi, C.; van Vuuren, D.P.; Eyring, V.; Friedlingstein, P.; Hurtt, G.; Knutti, R.; Kriegler, E.; Lamarque, J.-F.; Lowe, J.; et al. The Scenario Model Intercomparison Project (ScenarioMIP) for CMIP6. *Geosci. Model Dev.* **2016**, *9*, 3461–3482. [CrossRef]
18. Visioni, D.; MacMartin, D.G.; Kravitz, B.; Boucher, O.; Jones, A.; Lurton, T.; Martine, M.; Mills, M.J.; Nabat, P.; Niemeier, U.; et al. Identifying the sources of uncertainty in climate model simulations of solar radiation modification with the G6sulfur and G6solar Geoengineering Model Intercomparison Project (GeoMIP) simulations. *Atmos. Chem. Phys.* **2021**, *21*, 10039–10063. [CrossRef]
19. Seferian, R.; Nabat, P.; Michou, M.; Saint-Martin, D.; Voldoire, A.; Colin, J.; Decharme, B.; Delire, C.; Berthet, S.; Chevallieret, M.; et al. Evaluation of CNRM Earth System Model, CNRM-ESM2-1: Role of Earth System Processes in Present-Day and Future Climate. *J. Adv. Model. Earth Sys.* **2019**, *11*, 4182–4227. [CrossRef]
20. Boucher, O.; Servonnat, J.; Albright, A.L.; Aumont, O.; Balkanski, Y.; Bastrikov, V.; Bekki, S.; Bonnet, R.; Bony, S.; Bopp, L.; et al. Presentation and Evaluation of the IPSL-CM6A-LR Climate Model. *J. Adv. Model. Earth Sys.* **2020**, *12*, 2019MS002010. [CrossRef]
21. Mauritsen, T.; Bader, J.; Becker, T.; Behrens, J.; Bittner, M.; Brokopf, R.; Brovkin, V.; Claussen, M.; Crueger, T.; Esch, M.; et al. Developments in the MPI-M Earth System Model version 1.2 (MPI-ESM1.2) and Its Response to Increasing CO_2. *J. Adv. Model. Earth Syst.* **2019**, *11*, 998–1038. [CrossRef]
22. Sellar, A.; Jones, C.G.; Mulcahy, J.P.; Tang, Y.; Yool, A.; Wiltshire, A.; O'Connor, F.M.; Stringer, M.; Hill, R.; Palmieri, J.; et al. UKESM1: Description and Evaluation of the U.K. Earth System Model. *J. Adv. Model. Earth Sys.* **2019**, *11*, 4513–4558. [CrossRef]
23. Dola, S.S.; Bahsar, K.; Islam, M.; Sarker, M.M.R. Hydrogeological Classification and the Correlation of Groundwater Chemistry with Basin Flow in the South-Western Part of Bangladesh. *J. Bangladesh Acad. Sci.* **2018**, *42*, 41–54. [CrossRef]
24. Jayasree, V.; Venkatesh, B. Analysis of Rainfall in Assessing the Drought in Semi-arid Region of Karnataka State, India. *Water Res. Manag.* **2015**, *29*, 5613–5630. [CrossRef]
25. Washington, R.; Todd, M.; Middleton, N.J.; Goudie, A.S. Dust storm source areas determined by the Total Ozone Monitoring Spectrometer and surface observations. *Ann. Assoc. Am. Geogr.* **2003**, *93*, 297–313. [CrossRef]
26. Mbah, M.F.; Shingruf, A.; Molthan-Hill, P. Policies and practices of climate change education in South Asia: Towards a support framework for an impactful climate change adaptation. *Clim. Action* **2022**, *1*, 28. [CrossRef]